Soft-Switched PFC Boost Rectifier with Integrated ZVS Two-Switch Forward Converter

Yungtaek Jang, Dave L. Dillman, and Milan M. Jovanović

Delta Products Corporation
Power Electronics Laboratory
P.O. Box 12173, 5101 Davis Drive
Research Triangle Park, NC 27709

Abstract — **A soft-switched continuous-conduction-mode boost PFC front-end converter with an integrated zero-voltage-switched two-switch forward second-stage converter is introduced. In the proposed approach, a single transformer is commonly used by the two stages to provide isolation of the power supply and soft switching of all semiconductor switches including a controlled di/dt turn-off rate of the boost rectifier. The performance of the proposed approach was evaluated on a 150-kHz, 430-W/12-V, universal-line range prototype converter.**

I. Introduction

A boost power-factor-corrected (PFC) front-end converter followed by a dc-dc two-switch forward converter is one of the most extensively employed converter combinations in off-line power supplies used in low-end computer servers and high-end desk top computers. The front-end boost rectifier is employed to reduce the line-current harmonics and to provide compliance with various worldwide specifications governing the harmonic limits of the line current in off-line power supplies, whereas the two-switch forward converter is employed to provide galvanic isolation and tight output voltage regulation. The popularity of the two-switch forward converter topology stems from its maturity, simplicity, robustness, good performance, and low cost.

The continuous-conduction-mode (CCM) boost converter is the preferred topology for implementation of a front end with PFC over the range of medium to high power. In recent years, significant efforts have been made to improve the performance of high-power CCM boost converters [1]-[5]. The majority of these development efforts have been focused on reducing the adverse effects of the reverse-recovery characteristic of the boost diode on the conversion efficiency and electromagnetic compatibility (EMC) [6]. Similar effort has been put in optimizing and improving the performance of the two-switch forward converter [7]-[8].

In this paper, a novel ac-dc converter that integrates the CCM boost front end with the dc-dc two-switch forward converter is described. The integration of the two power stages is achieved by a magnetic component that is shared by both stages. This approach not only reduces the number of magnetic components, but also makes it possible to achieve a fully soft-switched ac-dc converter. Namely, in the integrated circuit, not only are the switches in the PFC boost converter soft switched, the switches in the two-switch forward converter are also able to achieve soft switching.

II. Soft-Switched PFC Boost Converter with Integrated Two-Switch Forward Converter

The proposed soft-switched PFC boost converter with integrated two-switch forward converter is shown in Fig. 1. The boost converter consists of voltage source V_{IN}, boost inductor L_B, main switch S, boost rectifier D, energy-storage capacitor C_B, and the active snubber circuit formed by auxiliary switch S_1, winding N_1 of transformer TR, snubber inductor L_S, and blocking diode D_1. The two-switch forward converter consists of switches S_{D1} and S_{D2} with associated antiparallel diodes, isolation transformer TR, rectifiers D_{R1} and D_{R2}, output inductor L_F, and output capacitor C_F.

To facilitate the explanation of the circuit operation, Fig. 2 shows a simplified circuit diagram of the proposed converter in Fig. 1. In the simplified circuit, energy-storage capacitor C_B is modeled by voltage source V_B by assuming that the value of C_B is large enough so that the voltage ripple across the capacitor is small in comparison to its dc voltage. In addition, boost inductor L_B and output filter inductor L_F are modeled as constant current sources I_{IN} and I_O, respectively, by assuming that the inductance of L_B and L_F are large so that during a switching cycle the currents through L_B and L_F do

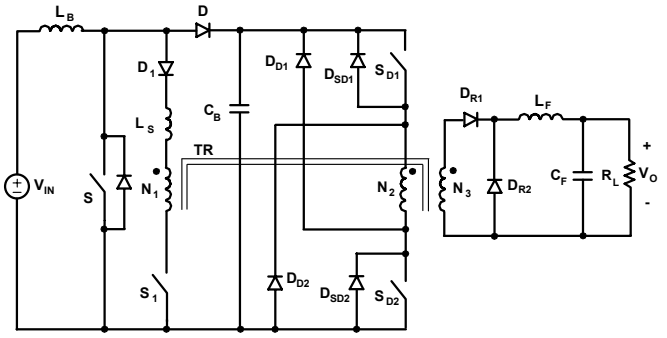

Fig. 1. Soft-switched power supply that integrates boost converter and two-switch forward converter.

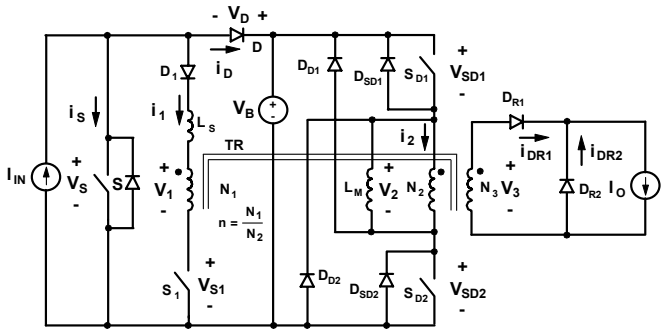

Fig. 2. Simplified circuit diagram along with reference directions of key currents and voltages.

not change significantly.

In this analysis, the leakage inductance of the transformer is neglected because it does not have a significant effect on the operation of the circuit. Moreover, since snubber inductor L_S and primary winding N_1 of transformer TR are connected in series, the leakage inductance of the transformer is absorbed by L_S. As a result, transformer TR is modeled by magnetizing inductance L_M and the three-winding ideal transformer. Finally, it is assumed that in the on state, the semiconductors exhibit zero resistance, *i.e.*, they are short circuits. However, the output capacitance of the switches, as well as the junction capacitance and the reverse-recovery charge of the boost rectifier are not neglected in this analysis.

To further facilitate the analysis of operation, Fig. 3 shows the major topological stages of the circuit in Fig. 1 during a switching cycle, whereas Fig. 4 shows its key waveforms. The reference directions of currents and voltages plotted in Fig. 4 are shown in Fig. 2.

As can be seen from the timing diagrams in Figs. 4(a), (b), and (c), the turn on of boost switch S and of forward switches S_{D1} and S_{D2} are synchronized, whereas auxiliary switch S_1 is turned on prior to the turn on of switches S, S_{D1}, and S_{D2}. In addition, auxiliary switch S_1 is turned off before boost switch S or forward switches S_{D1} and S_{D2} are turned off, *i.e.*, the proposed circuit operates with overlapping gate drive signals for the active snubber switch and the converter switches.

Prior to the turn on of switch S_1 at $t=T_0$, all switches are open. As a result, the entire input current I_{IN} flows through boost rectifier D into energy-storage capacitor C_B in the boost power stage, while output current I_O flows through output rectifier D_{R2} in the two-switch forward power stage as shown in Fig. 3(j). Because output rectifier D_{R2} is conducting during this period, voltage v_3 and induced voltage v_1 across winding N_1 of transformer TR is zero, *i.e.*, $v_1=(N_1/N_3)v_3=0$. After switch S_1 is turned on at $t=T_0$, the voltage of energy-storage-capacitor V_B is applied across snubber inductor L_S so that current i_1 starts to increase linearly, as illustrated in Fig. 4(g). The slope of current i_1 is

$$\frac{di_1}{dt}=\frac{V_B}{L_S}. \tag{1}$$

As current i_1 starts flowing through winding N_1 of transformer TR, the current in winding N_3 also begins to increase, *i.e.*, $i_{DR1}=(N_1/N_3)i_1$, as shown in Fig. 3(a) and Fig. 4(l). Because output current I_O is constant and equal to the sum of rectifier currents i_{DR1} and i_{DR2}, rectifier current i_{DR2} decreases until it becomes zero when rectifier current i_{DR1} increases. When rectifier current i_{DR2} becomes zero at $t=T_1$, output rectifier D_{R2} turns off, as shown in Fig. 4(m). Since the current through winding N_3 and rectifier D_{R1} is equal to output current I_O after the turn-off of D_{R2}, the increasing current in winding N_1 makes current i_2 in winding N_2 begin to flow. This current discharges the output capacitances of forward switches S_{D1} and S_{D2}, as illustrated in Fig. 3(b) and Fig. 4(i). During this period, voltage v_2 across winding N_2 of transformer TR starts to increase. After the output capacitances of forward switches S_{D1} and S_{D2} are fully discharged, switch currents i_{SD1} and i_{SD2} continue to flow through the antiparallel diodes of forward switches S_{D1} and S_{D2}, as shown in Fig. 3(c) and Fig. 4(i). To achieve ZVS of forward switches S_{D1} and S_{D2}, switches S_{D1} and S_{D2} should be turned on while their antiparallel diodes are conducting. To simplify the control circuit timing diagram, the turn-on of forward switches S_{D1} and S_{D2} is synchronized with the turn-on of boost switch S. While the antiparallel diodes of forward switches S_{D1} and S_{D2} are conducting, voltage v_2 across winding N_2 is equal to V_B so that induced voltage v_1 on winding N_1 is

$$v_1=\frac{N_1}{N_2}V_B=nV_B. \tag{2}$$

Because v_1 is constant, voltage applied across snubber inductor L_S is also constant so that current i_1 increases linearly with a slope of

$$\frac{di_1}{dt}=\frac{V_B-v_1}{L_S}=\frac{V_B-nV_B}{L_S}=(1-n)\frac{V_B}{L_S}. \tag{3}$$

During the same period, magnetizing inductance i_M increases with a slope given by

$$\frac{di_M}{dt}=\frac{V_B}{L_M}. \tag{4}$$

As current i_1 linearly increases, boost rectifier current i_D linearly decreases at the same rate since the sum of i_1 and i_D is equal to constant input current I_{IN}, *i.e.*, $i_1+i_D=I_{IN}$. Therefore, in the proposed circuit, the turn-off rate of the boost rectifier

$$\frac{di_D}{dt}=-(1-n)\frac{V_B}{L_S} \tag{5}$$

can be controlled by the proper selection of the inductance value of snubber inductor L_S and turns ratio n of transformer TR. Typically, for today's fast-recovery rectifiers, the turn-off rate di_D/dt should be kept around 100 A/μs. With the selected turn-off rate, the reverse-recovery current of the

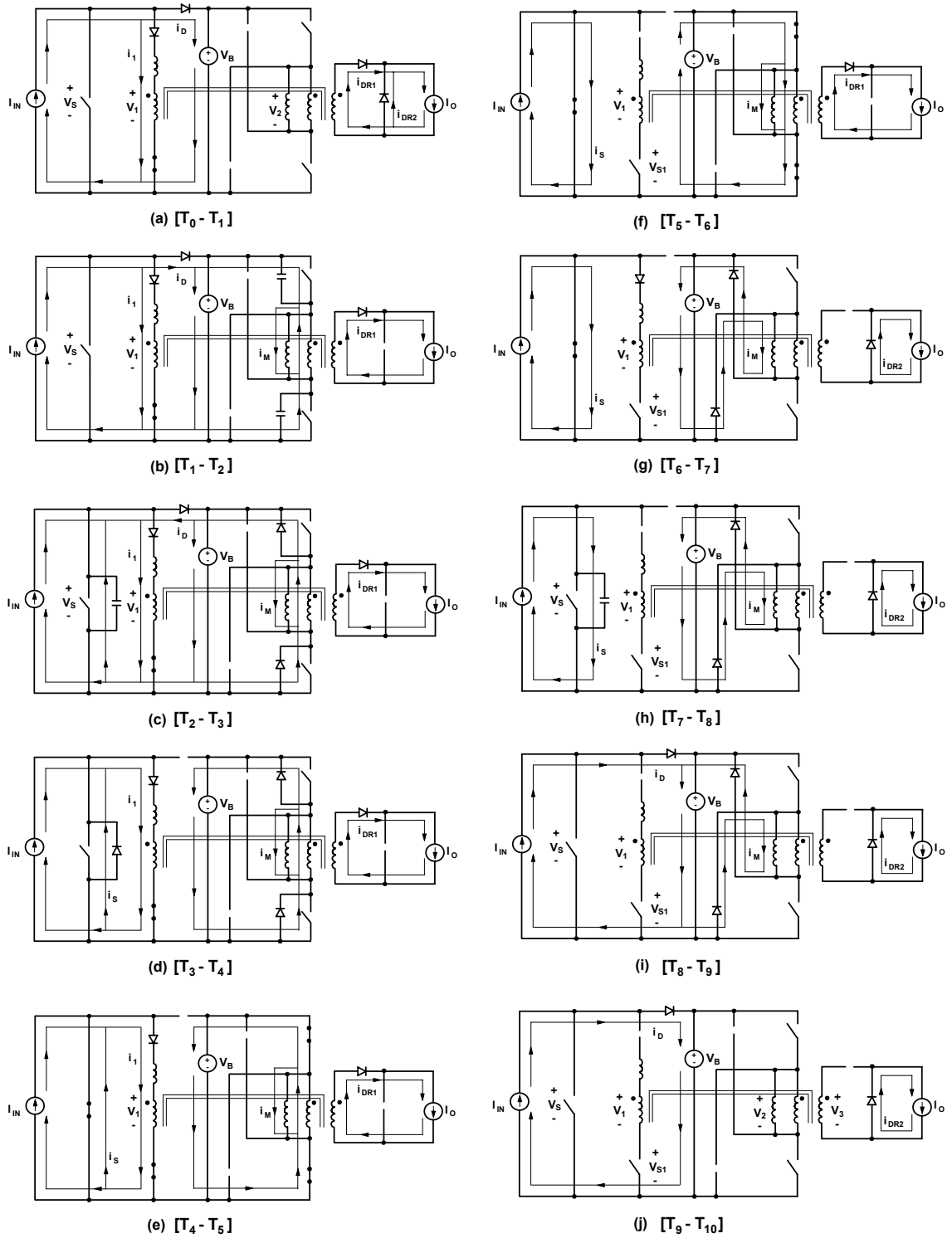

Fig. 3. Topological stages.

rectifier and the related power losses and EMI problems are minimized.

After $t=T_2$, current i_1 starts to discharge the output capacitance of boost switch S and charge the junction capacitance of boost rectifier D, as shown in Fig. 3(c). If the turns ratio of transformer TR is selected so that $n<0.5$, the energy stored in L_S is sufficient to completely discharge the output capacitance of boost switch S regardless of the load

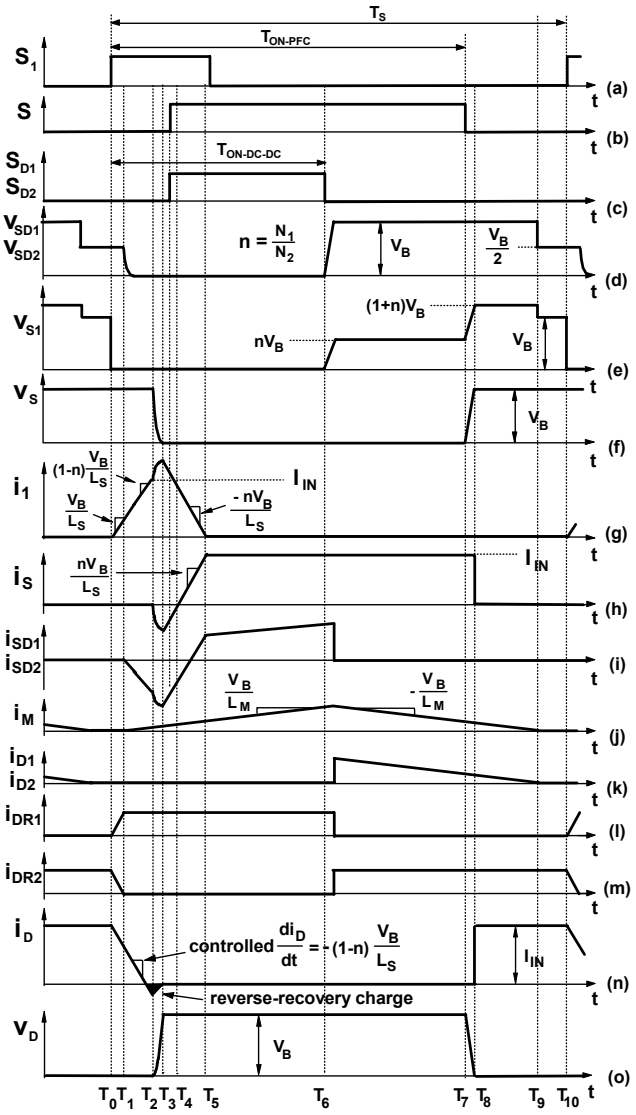

Fig. 4. Key waveforms.

and line conditions. Once the capacitance is fully discharged at t=T_3, current i_S continues to flow through the antiparallel diode of boost switch S, as shown in Fig. 3(d) and Fig. 4(h). During this period, voltage v_1 is applied in the negative direction across snubber inductor L_S. Therefore, current i_1 starts to decrease linearly at the rate given by

$$\frac{di_1}{dt} = -\frac{nV_B}{L_S}, \tag{6}$$

as illustrated in Fig. 4(g). The current in auxiliary switch S_1 also starts to decrease, whereas boost-switch current i_S starts to increase from the negative peak value, as shown in Figs. 4(g) and (h). To achieve ZVS of boost switch S, it is necessary to turn on boost switch S before its current becomes positive at t=T_4, *i.e.*, during the period when current i_S still flows through the antiparallel diode of switch S, as illustrated in Fig. 4(h).

As shown in Fig. 4(g), current i_1 continues to decrease until it reaches zero at t=T_5. Shortly after t=T_5, auxiliary switch S_1 is turned off to achieve zero-current switching (ZCS). After switch S_1 is turned off, the entire input current I_{IN} flows through boost switch S. As a result, the front-end boost converter stage is completely decoupled from the two-switch forward converter stage, as shown in Fig. 3(f). For the rest of the switching cycle, the two-switch forward converter stage continues to operate as a conventional two-switch forward converter.

After forward switches S_{D1} and S_{D2} are turned off at t=T_6, magnetizing current i_M starts to charge the output capacitances of forward switches S_{D1} and S_{D2}. When voltages v_{SD1} and v_{SD2} reach V_B, the magnetizing current is diverted from forward switches S_{D1} and S_{D2} to clamp diodes D_{D1} and D_{D2}, as shown in Fig. 3(g). At the same time, the reset of the transformer is initiated by bulk voltage V_B applied across winding N_2. During the reset time of the transformer, forward switch voltages v_{SD1} and v_{SD2} are equal to V_O, whereas the voltage across auxiliary switch S_1 is nV_B due to the magnetic coupling of windings N_1 and N_2, as illustrated in Figs. 4(d) and (e).

After boost switch S is turned off at t=T_7, voltage across switch S starts to increase linearly because constant input current I_{IN} begins charging the output capacitance of boost switch S, as shown in Fig. 3(h). The increasing boost-switch voltage causes an equal increase of voltage v_{S1} across auxiliary switch S_1. When boost-switch voltage v_S reaches V_B at t=T_8, boost diode D begins to conduct, as shown in Fig. 3(i). At the same time, auxiliary-switch voltage v_{S1} reaches its maximum value of $(1+n)V_B$. The circuit stays in the topological stage shown in Fig. 3(i) until magnetizing current i_M decreases to zero at t=T_9. The next switching cycle is initiated at t=T_{10}.

In summary, the major feature of the proposed circuit in Fig. 1 is the soft-switching of all semiconductor devices. Specifically, boost switch S and forward switches S_{D1} and S_{D2} are turned on with ZVS, whereas auxiliary switch S_1 is turned off with ZCS. In addition, boost diode D is turned off with a controlled turn-off rate of its current. Because all semiconductor components of the proposed converter operates with soft switching, the overall switching losses are minimized, which maximizes the conversion efficiency. In addition, soft switching has a beneficial effect on EMI and may result in a smaller size input filter [6].

However, it should be noted that complete ZVS of forward switches S_{D1} and S_{D2} can only be achieved if input current I_{IN} is large enough to produce a negative current through primary winding N_2 and discharge the output capacitances of switches S_{D1} and S_{D2} completely, as shown in Fig. 3(b). According to Fig. 3(b), to have a negative current flowing through winding N_2 after t=T_1, reflected current i_1 into winding N_3 has to be greater than output current I_O. If this

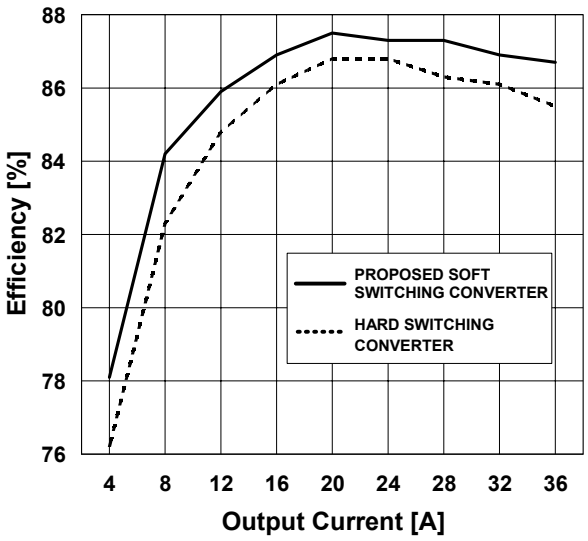

Fig. 5. Measured efficiency of 150 kHz, 430-W experimental converter with (dashed line) hard switching and (solid line) soft switching at V_{IN}=90 V_{AC}, V_B=380 V, and V_O=12 V as functions representing output current.

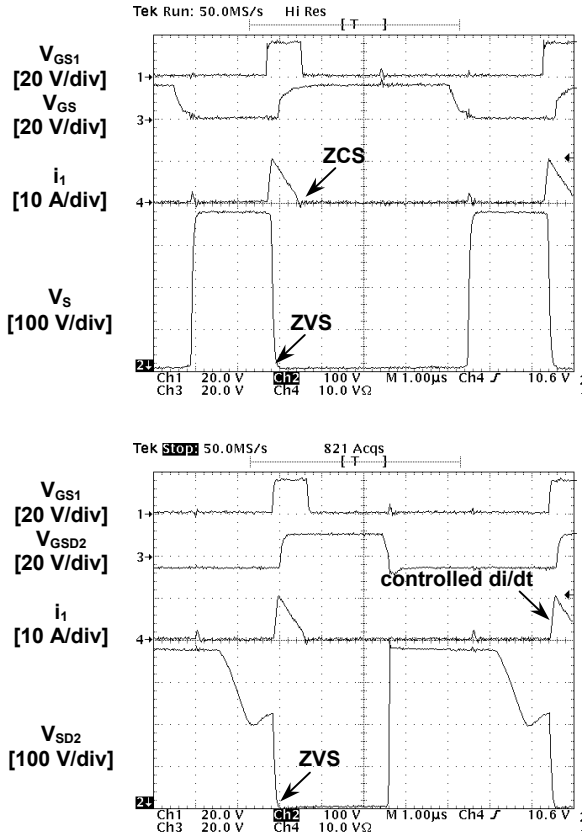

Fig. 6. Measured waveforms of experimental circuit at V_{IN}=90 V, V_B=380 V, I_O= 26 A, V_O=12 V. Time base: 1 µs/div.

condition is not met, forward switches S_{D1} and S_{D2} operate with partial ZVS. This mode of operation typically occurs near the zero crossing of the line voltage in a PFC boost converter. Since the input current is proportional to the line voltage, input current I_{IN} is small near the zero crossing of the line voltage. However, by adding an extra capacitor across boost switch S, forward switches S_{D1} and S_{D2} can achieve complete ZVS near the zero crossing of the line voltage.

Due to the ZVS of boost switch S and forward switches S_{D1} and S_{D2}, the most suitable switch component is a MOSFET (Metal Oxide Semiconductor Field Effect Transistor) device. Similarly, due to the ZCS of auxiliary switch S_1, an IGBT (Insulated Gate Bipolar Transistor) is suitable for the auxiliary switch.

In the proposed circuit, the voltage stresses on boost switch S, forward switches S_{D1} and S_{D2}, and boost rectifier D are identical to the corresponding stresses in the conventional converters. However, the voltage stress of auxiliary switch S_1 is

$$v_{S1(MAX)} = (1+n)V_B \,. \qquad (7)$$

The control of the proposed circuit is performed by two independent controllers that are synchronized. Specifically, one controller is used to regulate the output voltage of the front-end boost stage, *i.e.*, voltage V_B across the energy-storage capacitor C_B. The other controller is used to regulate output voltage V_O of the two-switch forward converter.

III. Experimental Results

The performance of the proposed converter was evaluated on a 430-W prototype circuit that was designed to operate from a universal ac line input and deliver up to 36 A at 12 V output. Switches S, S_1, S_{D1}, and S_{D2} operate at 150 kHz.

The experimental circuit was implemented with the following components: boost switch S and two-switch forward switches S_{D1} and S_{D2} – SPP20N60C2; auxiliary switch S_1 – SPA11N80C3; boost diode D and snubber diode D_1 – RHRP1560; output diodes D_{R1} and D_{R2} – S60SC6M; bulk capacitor C_B – 470 uF/450 V; and output capacitor C_F – 2 × 2200 uF/16 V.

To build boost inductor L_B, a toroidal core (MS130060) from Arnold and 71 turns of magnet wire (AWG #19) were used. External snubber inductor L_S was connected in series with the auxiliary winding of transformer TR, as shown in Fig. 1. The required inductance is approximately 2.7 µH at full load. Snubber inductor L_S was built using a toroidal core (A189043) and 9 turns of magnet wire (AWG #19). Transformer TR was built using a pair of ferrite cores (PJ40-3C94). Three magnet wires (N_1=7 turns : N_2=26 turns : N_3=2 turns) were used.

Figure 5 shows the measured efficiencies of the experimental converter with (solid lines) and without (dashed lines) the active snubber circuit as functions representing output current. As can be seen in Fig. 5, the active snubber

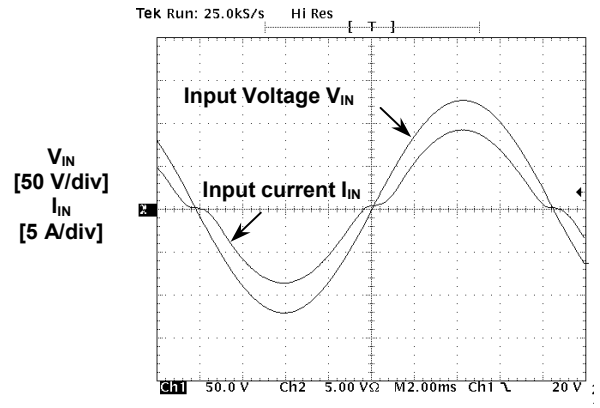

Fig. 7. Measured waveforms of experimental circuit at V_{IN}=90 V, V_B=380 V, I_O= 36 A, V_O=12 V. Time base: 2 ms/div.

improves the conversion efficiency in the entire measured power range. The active snubber improves the efficiency by approximately 1.5% at full load.

Figures 6 and 7 show the oscillograms of key waveforms in the experimental converter. As can be seen from the corresponding waveforms in Fig. 4, there is a good agreement between the experimental and theoretical waveforms. As can be seen from Fig. 6, switches S and S_{D2} are turned on with ZVS since their voltages V_S and V_{SD2} fall to zero before gate-drive signals V_{GS} and V_{GSD2} become high. Moreover, auxiliary switch S_1 achieves soft-switching turn off because switch current i_1 becomes zero before auxiliary switch S_1 is turned off. Also, it should be noted that the rising slope of current i_1 is approximately di_1/dt = 80 A/μs which is proportional to boost diode current i_D during the period when boost diode D is turned off as shown in Fig. 6. The reverse-recovery loss of boost diode D is dramatically reduced by the controlled di_D/dt. Figure 7 shows the ac waveforms of input voltage V_{IN} and input current I_{IN}. The power factor of input current I_{IN} is higher than 99%.

IV. Summary

A soft-switched boost PFC front-end converter with an integrated ZVS two-switch forward second-stage converter has been introduced. By using a single magnetic device which is mutually shared by the PFC boost converter and the two-switch forward converter, boost switch S and forward switches S_{D1} and S_{D2} are turned on with ZVS, auxiliary switch S_1 is turned off with ZCS, and boost diode D is turned off softly using a controlled di/dt rate. As a result, the turn-on switching losses in the boost and forward switches, the turn-off switching loss in the auxiliary switch, and reverse-recovery-related losses in the boost diode are eliminated, which maximizes the conversion efficiency. The performance of the proposed approach was evaluated on a 150-kHz, 430-W, universal-line range prototype converter delivering 12-V/36-A output. The proposed technique improves the efficiency by approximately 1.5% at full load.

References

[1] D.C. Martins, F.J.M. de Seixas, J.A. Brilhante, I. Barbi, "A family of dc-to-dc PWM converters using a new ZVS commutation cell," *IEEE Power Electronics Specialists' Conf. (PESC) Rec.*, pp. 524 - 530, June 1993.

[2] G. Moschopoulos, P. Jain, G. Joós, "A novel zero-voltage switched PWM boost converter," IEEE *Power Electronics Specialists' Conf. (PESC) Rec*., pp. 694-700, 1995.

[3] J.-H. Kim, D.Y. Lee, H.S. Choi, B.H. Cho, "High performance boost PFP (power factor pre-regulator) with an improved ZVT (Zero Voltage Transition) converter," *IEEE Applied Power Electronics (APEC) Conf. Proc.*, pp. 337-342, 2001.

[4] F.T. Wakabayashi, M.J. Bonato, C.A. Canesin, "Novel high-power factor ZCS-PWM preregulators," *IEEE Trans. Industrial Electronics, vol. 48, no. 2*, pp. 322-333, Apr. 2001.

[5] H.S. Choi, B.H. Cho, "Zero-current-switching (ZCS) power factor pre-regulator (pfp) with reduced conduction losses," *IEEE Applied Power Electronics (APEC) Conf. Proc.*, pp. 962 -967, 2002.

[6] H. Chung, S.Y.R. Hui, K.K. Tse, "Reduction of Power Converter EMI Emission Using Soft-Switching Technique," *IEEE Trans. Electromagnetic Compatibility, vol. 40, no. 3*, pp. 282-287, Aug. 1998.

[7] A.P. Patel "Forward Converter Circuit Having Reduced Switching Losses," US Patent 6,370,051B1, April 9, 2002.

[8] G. Huang, Y. Gu, Z. Liu, and A.J. Zhang "Resonant Reset Dual Switch Forward Dc-to-Dc Converter," US Patent 6,469,915B2, October 22, 2002.